Reactivity of the nitrogen-centered tryptophanyl radical in the catalysis of the radical SAM enzyme NosL

Haocheng Qianzhu, Wenjuan Ji, Xinjian Ji, Leixia Chu, Chuchu Guo, Wei Ding, Jiangtao Gao,* and Qi Zhang*

Instrumentation

High-performance liquid chromatography (HPLC) was performed using a Thermo Scientific Dionex Ultimate 3000 system with a diode array detector equipped with a C18 column (AccucoreXL C18, Thermo Scientific, 4.6 x 260 mm,1.8 um particle size). High resolution mass spectrometry (HR-MS) analysis was performed using a Q-Exactive™ Focus Hybrid Quadrupole-Orbitrap MassSpectrometer (Thermo Fisher) equipped with a Dionex Ultimate 3000 HPLC system (Thermo Fisher). NMR spectra were recorded using Bruker 400 MHz NMR spectrometer at the Nuclear Magnetic Resonance Facility at Fudan University. PCR was performed on a Bio-Rad T100™ Thermal Cycler using PrimeSTAR® HS DNA Polymerase (Takara Biotechnology Co. Ltd, China) or Phanta Max Super-Fidelity DNA Polymerase (Vazyme Biotech Co. Ltd, China).

Chemicals and Biochemicals

All chemical reagents and anhydrous solvents were purchased from commercial sources and used without further purification unless otherwise specified. S-adenosyl-L-methionine (SAM) were purchased from Sangon Biotech Co. Ltd (Shanghai, China). Deuterium oxide (99.9%), L-tryptophan methyl ester, 3-indoleethanol, 5′-chloro-5′-deoxyadenosine, and *p*-nitrothiophenol were from Sigma-Aldrich Co. Ltd (USA). L-Trp, sodium dithionite, $Fe(NH_4)_2(SO_4)_2 \cdot 6H_2O$ and Na_2S were from Adamas Reagent Co. Ltd (Shanghai, China). Sulfuryl chloride was from Energy Chemical Co. Ltd (Shanghai, China).

Construction of NosL-Y90F expression plasmid

The NosL Y90F mutant was constructed using the one-step site-directed mutagenesis method. PCR was performed by using a primer pair (5'-CCT TCG TGC CGC TCTTCA CCA CCA ACT

ACT GCG ACT CC-3' and 5'-GTT GGT GGT GAA GAG CGG CAC GAA GGT GTG CAG CCG GG-3', mutation sites are underlined), and plasmid NosL-pET28a constructed previously[1] as the PCR template. PCR was performed for 30 cycles with denaturation, annealing, and extension at 98 °C, 65 °C, and 72 °C, respectively. The PCR product (from 50 μL reaction mixture) was purified by agarose gel, redissolved in 20μL dd H_2O, and treated with 1 μL DpnI (NEB, 20,000 units/ml) at 37°C for 1 hr to digest the template DNA. 5 μL of the resulting mixture was used to transform chemically competent *E. coli* DH5α cells. The cells were plated on LB-agar containing kanamycin sulfate (50 μg/mL) for positive clones, which were confirmed by DNA sequencing.

Expression of NosL wild type and mutant enzymes

E. coli BL21 (DE3) cells were transformed via electroporation with each plasmid for protein expression. A single colony transformant was used to inoculate a 5 mL LB culture supplemented with 50 μg/mL kanamycin sulfate. The culture was grown at 37 °C (180 rpm) for 12 h and was used to inoculate 1 L of LB medium containing 50 μg/mL kanamycin sulfate. Cells were grown at 37 °C and 180 rpm to an OD_{600} 0.6-0.8, and IPTG was then added to a final concentration of 0.2 mM, and sterilized $Fe(NH_4)_2(SO_4)_2$ was added to a final concentration of 100 μM. After additional 18 h of incubation at 20 °C and 180 rpm, the cells were harvested by centrifugation at 5000 x g for 15 min at 4 °C. The pellet was used directly for protein purification or stored at −80 °C upon further use.

Preparation of the reconstituted NosL and mutant enzymes

Protein purification and [4Fe-4S] reconstitution were performed in an anaerobic glove box (Coy Laboratory Product Inc., USA) with less than 2 ppm of O_2. The cell pellet was resuspended in 20ml of the lysis buffer (50 mM MOPS, 200 mM NaCl, and 10% (v/v) glycerol, pH adjusted to 8.0 by 2M NaOH), and was lysed by sonication on ice. Cell debris was removed via centrifugation at 18, 000 x g for 30 min at 4 °C. The supernatant was incubated with 4 ml Ni-NTA resin pre-equilibrated with the lysis buffer, and then subjected to affinity purification on a column. The desired fractions were combined and concentrated using an Amicon Ultra-15 Centrifugal Filter

Unit and analyzed by SDS-PAGE (12%Tris-glycine gel). Protein concentration was determined using a Bradford Assay Kit (Bio Rad) using bovine serum albumin (BSA) as a standard.

For reconstitution of the [4Fe-4S] cluster, freshly prepared dithiothreitol (DTT) was added to the purified protein fraction to a final concentration of 5 mM. $Fe(NH_4)_2(SO4)_2$ solution (50 mM) was then added carefully to a final concentration of 500 μM. After 10 min of incubation at the room temperature, Na_2S solution (50 mM) was added in the same way to a final concentration of 500 μM. After further incubation on ice for 5-7 h, the resulting blackish solution was subjected to desalting on a PD-10 column (GE Healthcare) pre-equilibrated with the elution buffer I (50 mM MOPS, 25 mM NaCl, 10 mM DTT and 10% (v/v) glycerol, pH 8.0) or elution buffer II (50 mM Tris, 25 mM NaCl, 1 mM DTT, ～1.5%(v/v) glycerol, pD～8.0, ～98% D_2O). The protein fraction was collected and concentrated, and was used directly for in vitro assay or stored at −80 °C upon further use.

Enzyme assays in highly enriched D_2O

The D_2O buffer (elution buffer II, 50 mM Tris, 250 mM NaCl, 10 mM DTT, ～1.5%(v/v) glycerol, pD～8) was prepared by dissolve 60 mg (5 mM) Tris base, 15 mg (2.5 mM) NaCl, 1.5 mg (0.1 mM) DTT, and 100～200 μL glycerol in 10 ml deuterium oxide (99.9%). This buffer was used for protein desalting with a PD-10 column (GE Healthcare). After desalting, the target protein was concentrated, and mixed with an equal volume of elution buffer II. The resulting protein solution was further concentrated to a protein concentration of 80～100 μM and was used directly in biochemical analysis. By comparing with the hydroxylmethyl signal (δ = 3.38) of Tris, the H_2O concentration was estimated to be less than 2% in the resulting protein solution. A typical assay was carried out by sequential addition of 2 μL L-Trp solution (20 mM in D_2O), 2 μL SAM solution (50 mM in D_2O), 2 μL sodium dithionite solution (0.1 M in D_2O) into 150 μL protein solution. Reactions were maintained at room temperature (～25°C) for different time intervals and were quenched by addition of trichloroacetic acid (TCA) to a final concentration of 5% (v/v). After removal of the protein precipitates by centrifugation, the supernatant was subjected to LC-HRMS analysis.

HPLC analysis

HPLC analysis was performed using a C18 analytic column (Accucore XL C18, Thermo Scientific, 4.6 x 250 mm). The column was equilibrated with 85% solvent A (H_2O, 0.1% TFA) and 15% solvent B (CH_3CN, 0.1% TFA), and developed at a flow rate of 1 ml/min and UV detection at 254 nm and 280 nm: 0-3 min, constant 40% A / 50% B; 3-20 min, a linear gradient to 2% A / 98% B; 20-25min, constant 2% A / 98% B; 25-30min, a linear gradient to 40% A / 50% B. LC-MS analysis was performed using a similar elution program.

Density functional theory (DFT) and statistical mechanics calculations

DFT calculations[2, 3] were performed with the Gaussian 09 program.[4] The NosL reaction intermediates and transition states were calculated by using the unrestricted B3LYP[5, 6] and M06[7] hybrid functionals in parallel. Structure optimization was performed using the 6-31+G(d,p) basis set, and energies were calculated using the 6-311+G(2d,p) basis set. The optimized structures were checked with harmonic vibration frequency calculations. The solvent effect was estimated with IEFPCM calculation[8, 9] with radii and non-electrostatic terms for SMD solvation model[10] in water (ε = 78.4) and in ethanol (ε = 24.5). All the transition states have been validated by intrinsic reaction coordinate (IRC) calculation in both forward and reverse directions. Canonical orbitals were calculated using isosurface values of 0.04.

To investigate the dAdo radical-mediated hydrogen abstraction reactions, the dAdo radical is modeled as an ethyl radical and L-Trp is modeled as methylamine, in a way similar to a recent study on the radical SAM enzyme HydE.[11] Both geometry optimization and energy calculation were performed at the M06/6-311+G(2d,p)/SMD(water) level of theory. Statistical mechanics analysis were performed using the canonical transition-state theory (TST)[12] with Wigner tunneling correction (TSTW)[13] embedded in the KiSThelP software package.[14] The temperature was set to 298.00K and the atmospheric pressure to 1.0 bar without any artificial adjustment.

Molecular Mechanical Calculations

All protein models were prepared in Schrodinger suite software under the OPLS_2005 force field.[15] Hydrogen atoms were added to the repaired crystal structures at physiological pH (7.4)

with the PROPKA[16] tool to optimize the hydrogen bond network provided by the Protein Preparation tool in Schrodinger software. Constrained energy minimizations were conducted on the full-atomic models, with heavy atom coverage to 0.4 Å.

Chemical model reaction

1) Preparation of 4-nitrobenzenesulfenyl chloride (compound **2**)

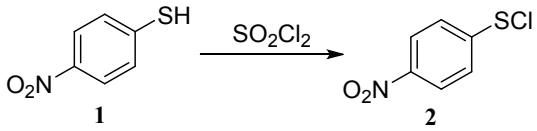

1 **2**

4-nitrobenzenesulfenyl chloride was synthesized according to a previously reported procedure.[17] Briefly, sulfuryl chloride (1.35g, 10.00mmol) was added dropwise to a solution of *p*-nitrophenol (compound **1**) (1.40g, 10.00mmol) in 20mL dichloromethane incubated in ice bath. The reaction mixture was stirred for 1 hr in ice bath, and was concentrated under vacuum to give the crude compound **2** (13.30g, 70%), which was used immediately in the next step.

2) Preparation of compound **4**

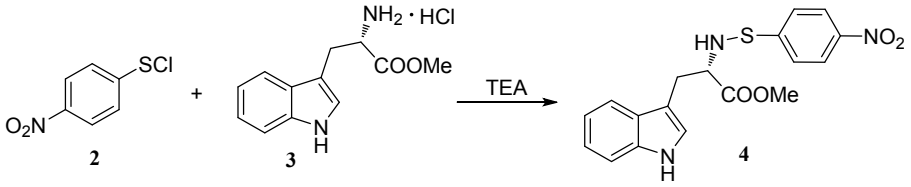

2 **3** **4**

Compound **4** was synthesized according to a procedure reported by Bowman *et al*.[18] Briefly, the crude compound **2** (0.21g, 1.10mmol) and methyl L-tryptophanate hydrochloride (**3**) (0.26g, 1.00mmol) was dissolved in 20 mL diethyl ether, and the solution was incubated in ice bath. 5 ml triethylamine (20μL, 1.10mmol) diethyl ether solution was added dropwise to the solution, and the resulting mixture was stirred for 1 hr before concentration under vacuum to give a yellow oil. The product was purified by preparation TLC plates to give compound **4** (180 mg, 49%). MS (ESI) $[M+H]^+$ calculated 372.1018, found 372.1010. ^1H NMR($CDCl_3$, 400MHZ) δ = 3.09-3.15 (dd, 1H, J_1 = 8.4Hz, J_2 = 13.8Hz), δ = 3.31-3.36 (dd, 1H, J_1 = 5.6Hz, J_2 = 14.2Hz), δ = 3.65 (s, 3H), 3.82-3.86 (m, 1H), 7.04~7.06 (d, 2H, J = 9.2Hz), 7.16-7.20 (m, 1H), 7.27-7.36 (m, 3H), 7.66~7.68 (d, H, J = 8.0Hz), 8.00~8.02 (d, 2H, J = 9.2Hz), 8.89 (s, 1H).

3) Photoreaction of **4**

Compound **4** (18 mg, 0.049 mmol) was dissolved in 10 mL acetonitrile and the solution was transferred to a small quartz tube reactor, which was irradiated for 1 hr under 254nm UV light. The resulting reaction mixture was directly analyzed by HPLC and was diluted 100-fold with acetonitrile before LC-HRMS analysis.

Fig. S1 DFT-calculated potential energy profile for the model study discussed in the main text. Energies were calculated at the B3LYP/6-311+G(2d,p)/SMD(water) level of theory with geometry optimized at the B3LYP/6-31+G(d,p)/SMD(water) level. This analysis shows that the energy profile for the fragmentation of tryptophan methyl ester is similar to that of tryptophan, thereby validating the chemical model study discussed in the main text (also see Fig. 3 in the main text and Fig S8, ESI† for comparison). All the transition states (shown in brackets) have been validated by intrinsic reaction coordinate (IRC) calculation in both forward and reverse directions. ΔG_{sol}, free energy of activation; ΔH_{sol}, enthalpy of activation.

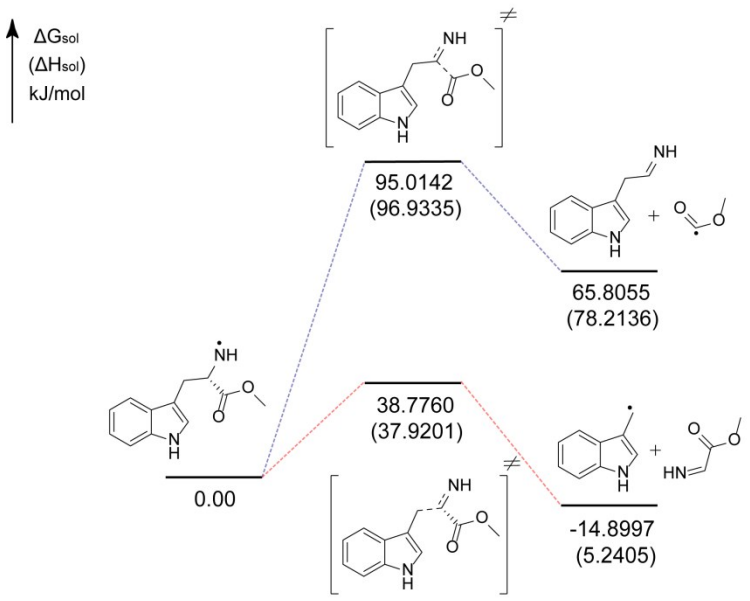

Fig. S2 UV spectra of X1 (a) and X2 (b), which are very similar to that of compound **4** (c).

a

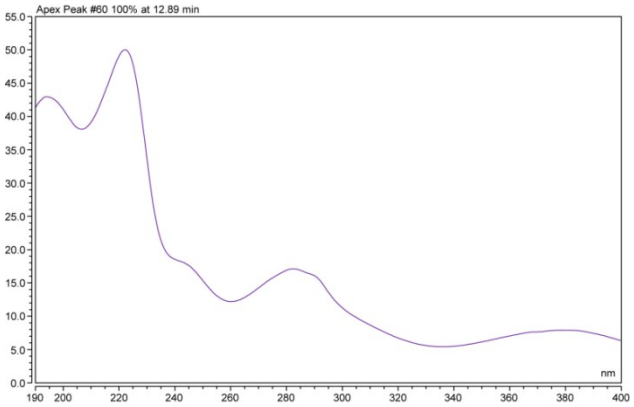

b

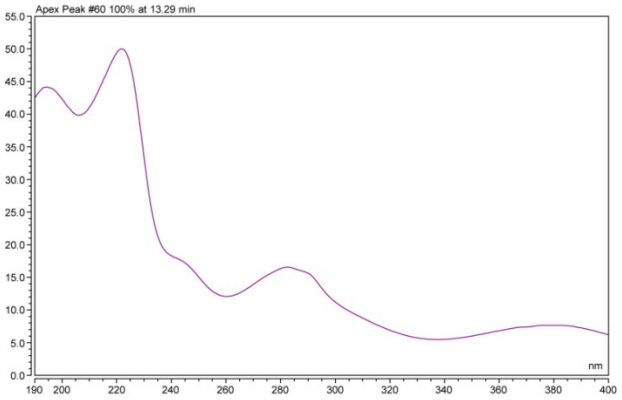

c

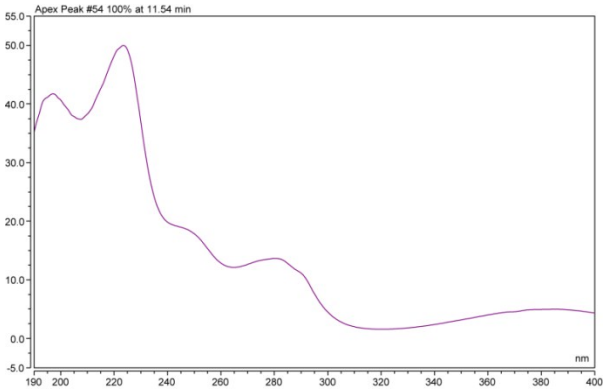

Fig. S3. Structural analysis of X1 and X2 by HR-MSMS, showing (a) the theoretical MS/MS fragmentation of X1 and X2, (b) the HRMS and HR-MS/MS spectra of X1, and (c) the HRMS and HR-MS/MS spectra of X2. The fragment ions that are also observed in the HR-MSMS spectrum of **4** are shown in blue. The characteristic ions (m/z = 283.05) of X1 and X2 are shown in red.

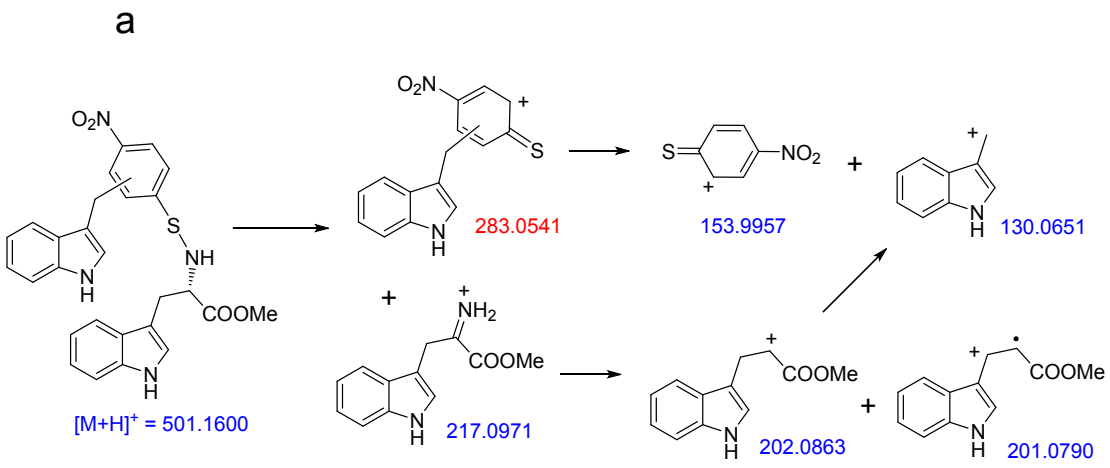

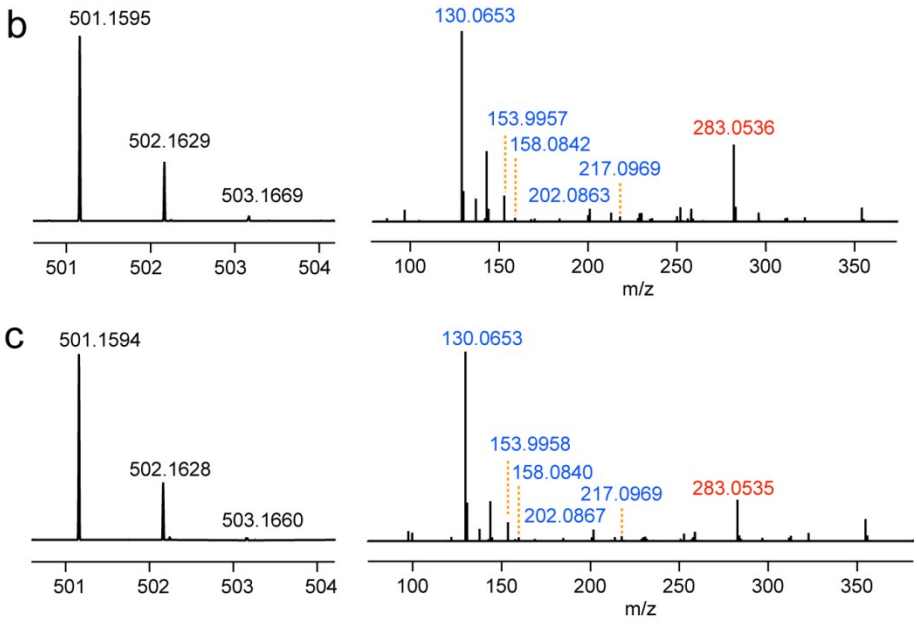

Fig. S4. HR-MSMS analysis of compound **4**, showing (a) the theoretical MS/MS fragmentation of **4**, and (b) the HR-MS/MS spectrum.

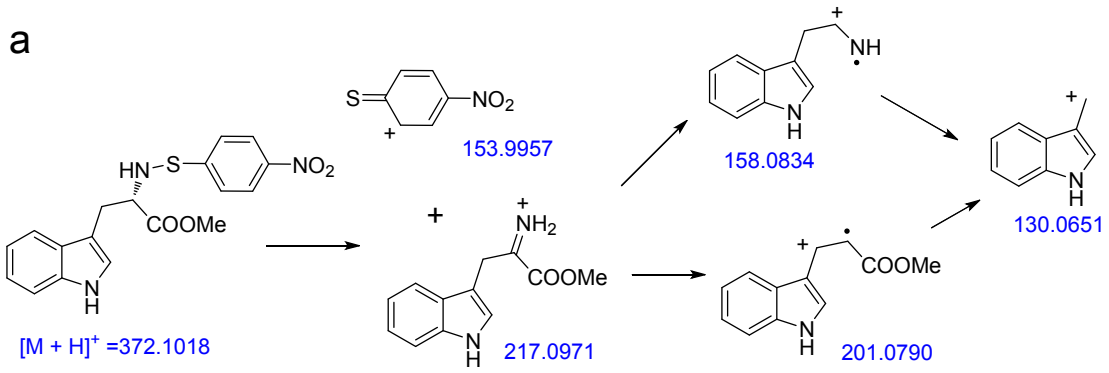

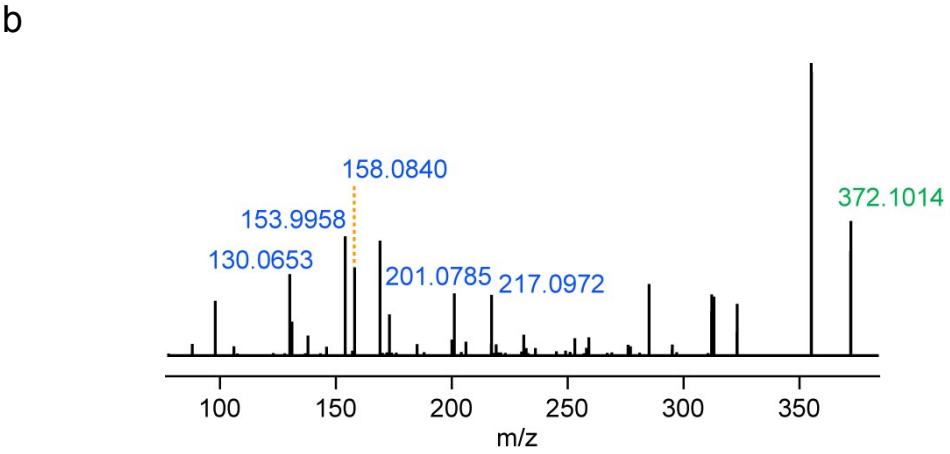

Fig. S5. Orbital analysis and regioselectivity prediction of the radical addition of **3** to **4**. The energy difference between HOMO of **3** and LUMO of **4** (0.06085 Hartree) is smaller than that between HOMO of **4** and LUMO of **3** (0.15019 Hartree), suggesting that **3** should specifically attack the nitrophenyl moiety of **4** (where the LUMO electrons locate). Because in the LUMO of **4** the electrons locate on the nitro para-positions, not the meta-positions, addition of **3** to **4** should mainly occur on the nitro para-positions. Canonical orbitals were calculated using isosurface values of 0.04.

Compound **4:** **HOMO (-0.21706 Hartree)** **LUMO (-0.09964 Hartree)**

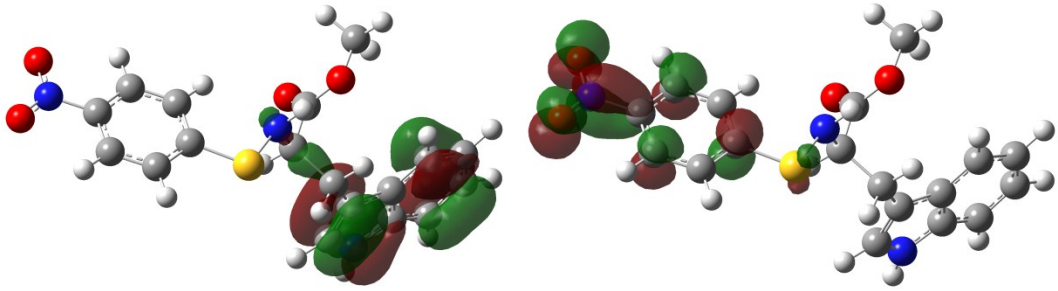

Radical **3:** **HOMO (-0.16049 Hartree)** **LUMO (-0.06687 Hartree)**

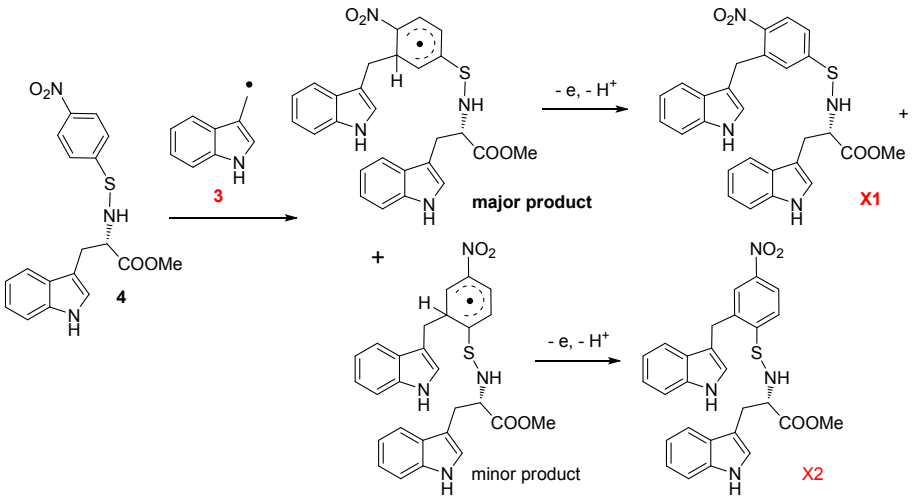

Fig. S6. Orbital analysis and regioselectivity prediction of the radical addition of **6** to **4**. The energy difference between HOMO of **4** and LUMO of **6** (0.01638 Hartree) is smaller than that between HOMO of **4** and LUMO of **3** (0.16195 Hartree), suggesting that **6** should specifically attack the indolyl moiety of **4** (where the HOMO electrons locate). Because in the HOMO of **4** the electrons equally locate on several atoms of the indole ring, a series of adduct isomers Y are expected, which is consistent with our LC-HRMS analysis (Y1, Y2, Y3 in the main text). Canonical orbitals were calculated using isosurface values of 0.04.

Compound **4:** **HOMO (-0.21706 Hartree)** **LUMO (-0.09964 Hartree)**

Radical **6:** **HOMO (-0.26159 Hartree)** **LUMO (-0.20068 Hartree)**

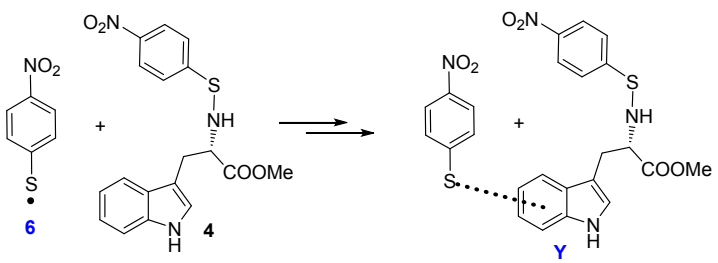

Fig. S7. Structural analysis of Y1, Y2, and Y3 by HR-MSMS, showing (a) the theoretical MS/MS fragmentation of Y1, Y2, and Y3, (b) the HR-MS/MS spectrum of Y1, (c) the HR-MS/MS spectrum of Y2, and (d) the HR-MS/MS spectrum of Y3. The fragment ions that are also observed in the HR-MSMS spectrum of **4** are shown in blue. The characteristic ions (m/z = 370.09 and 283.05) are shown in red.

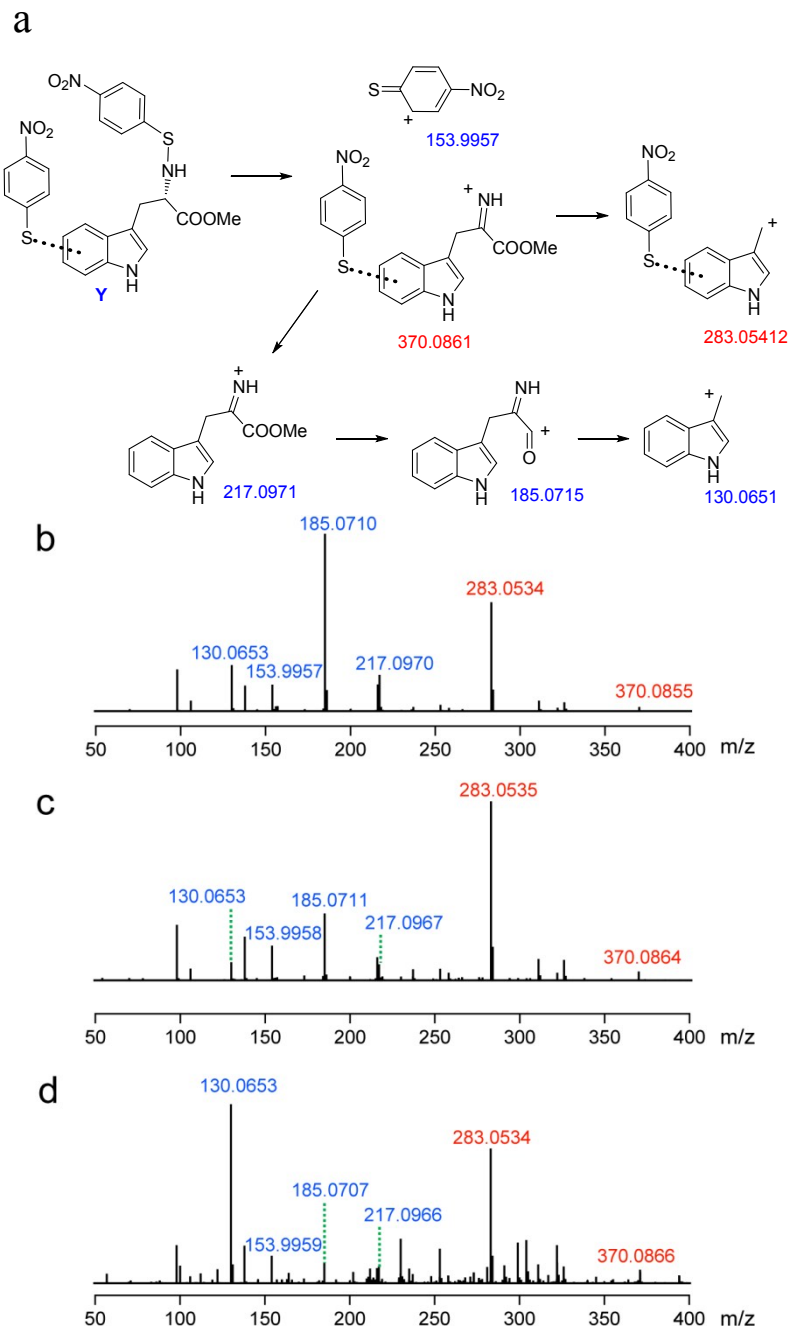

Fig. S8. Quantification for the cleavage products of the nitrogen-centered radical (**5** in the main text). Because 3-indoleacetaldehyde (IA) could be susceptible to oxidization, we treated the reaction mixture with an excess amount of $NaBH_4$ to reduce it to 3-indoleethanol, and the latter was quantified by comparing with the 3-indoleethanol standard. Because X1 and X2 share very similar UV-vis spectra with compound **4** (Fig. S2), these two compounds were quantified by the absorbances at 280 nm in HPLC and comparing with that of **4**. Less than 0.5% of **4** was transformed to X1 and X2 in this analysis. Production of 3-methylindole was quantified by comparing the UV absorbance in HPLC analysis with the 3-methylindole standard. Analysis was performed for two parallel reactions and the standard deviations (S.D.) are shown by the error bars.

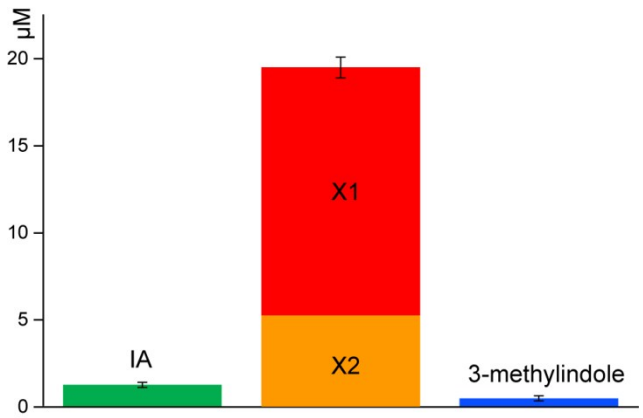

Fig. S9. DFT-calculated potential energy profiles in NosL catalysis. Energies were calculated at the levels of B3LYP/6-311+G(2d,p)/SMD(water), B3LYP/6-311+G(2d,p)/SMD(ethanol), and M06/6-311+G(2d,p)/SMD(water), respectively, with geometry optimized at the levels of B3LYP/6-31+G(d,p)/SMD(water), B3LYP/6-31+G(d,p)/SMD(ethanol), and M06/6-31+G(d,p)/SMD(water), respectively. These parallel calculations show similar trends of reaction energy. All the transition states have been validated by intrinsic reaction coordinate (IRC) calculation in both forward and reverse directions.

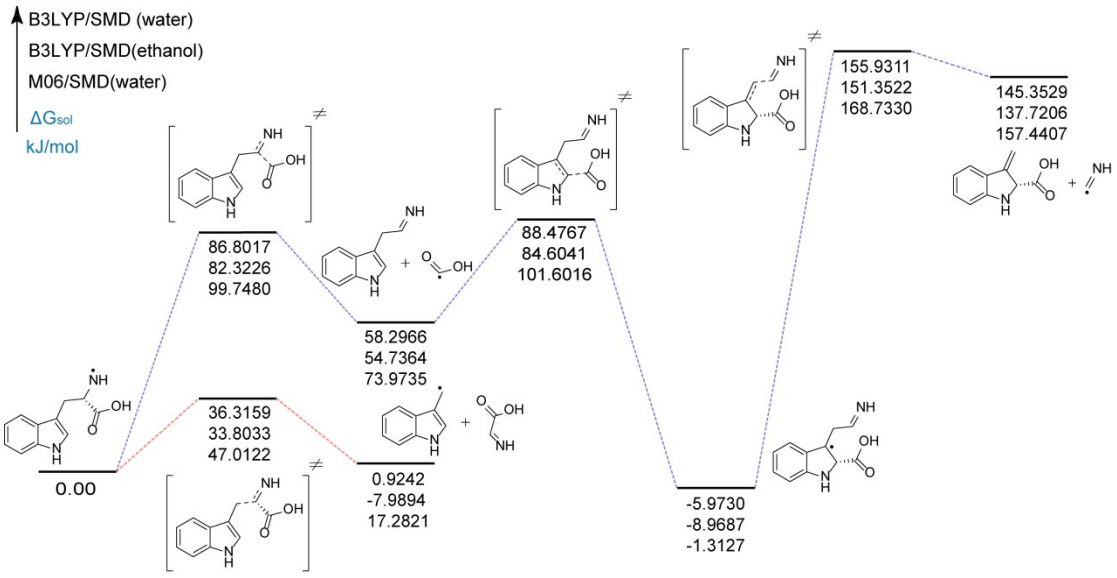

Fig. S10. Intrinsic reaction coordinate (IRC) calculation for the transition state structures in **Fig. 3** (main text) and in **Fig. S9**, showing that all the transition states connect the expected reactants and products along the IRC pathways. All stationary points were optimized at the B3LYP/6-31+G(d,p) level of theory.

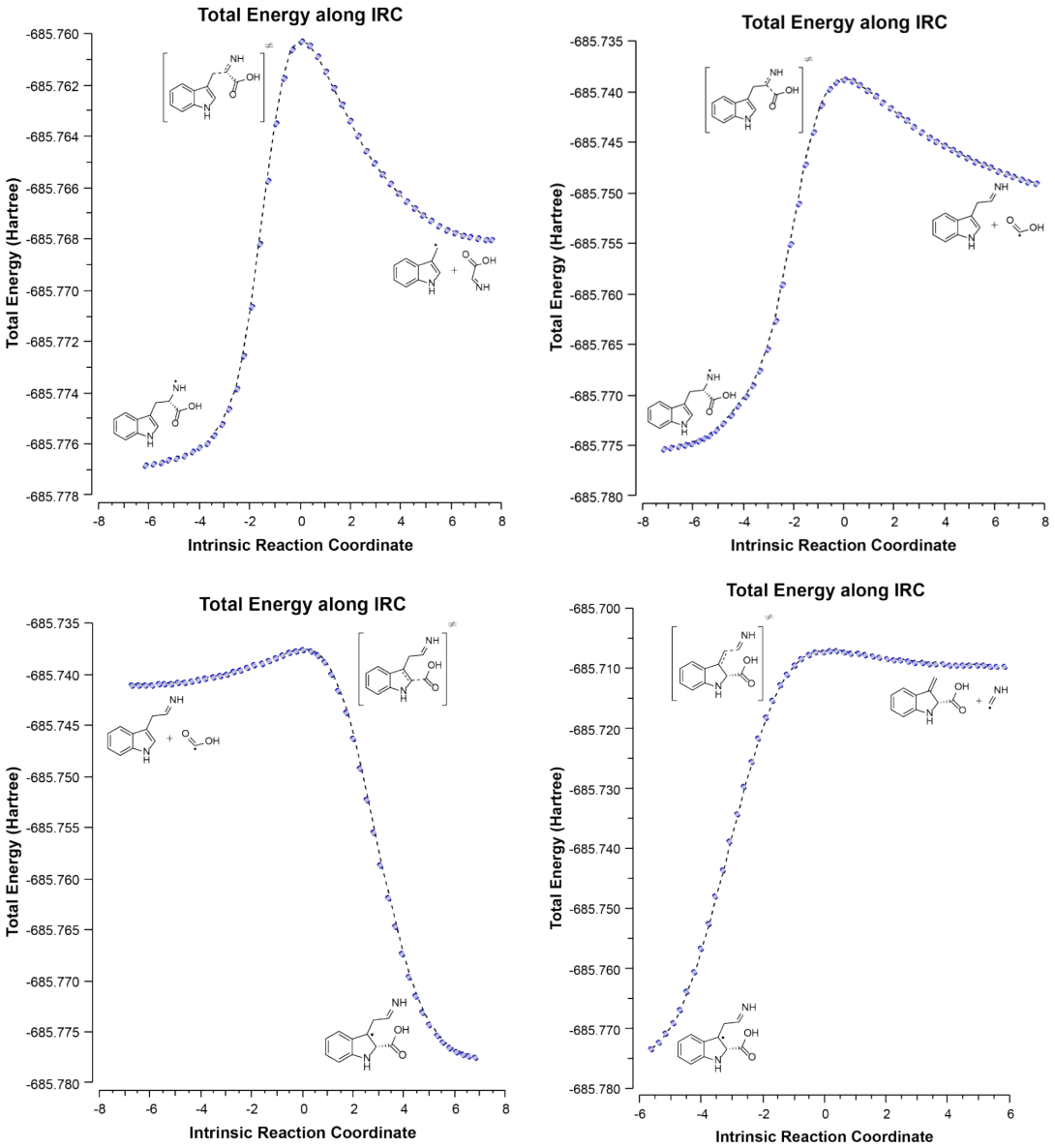

Fig. S11. A detailed kinetic model for the NosL-catalyzed reaction in D_2O. In the catalysis, the dAdo radical resulting from SAM cleavage abstracts a deuterium from the amino group with a rate constant of k_B to produce an amino-center radical (RND•), which proceeds via a β fragmentation (either Cα-Cβ or Cα-C scission) to produce corresponding products; this rate can be described by an apparent net rate constant k_{frag}. Alternatively, instead of β fragmentation, RND• can abstract a hydrogen back from the singly deuterated dAdoH that contain one deuterium and two protium atoms. As revealed by our DFT and statistical mechanics analysis (see **Fig. S12** and **Table S1**), protium abstraction by RND• (k_{-c}) is much faster that the reverse deuterium rebound process (k_{-B}), and the former results in a singly deuterated amino group (RNDH), which can be converted to the doubly deuterated amino group (RND_2) by a rapid solvent exchange process (k_{sol}) for the next round of dAdo radical-mediated hydrogen abstraction. dAdo radical can also be reduced by a hydrogen equivalent that can be described by an apparent rate constant k_{quen}. The hydrogen equivalent that quenches the dAdo radical could come from either a solvent-nonexchangeable or solvent-exchangeable site with a ratio of χ/(1-χ).

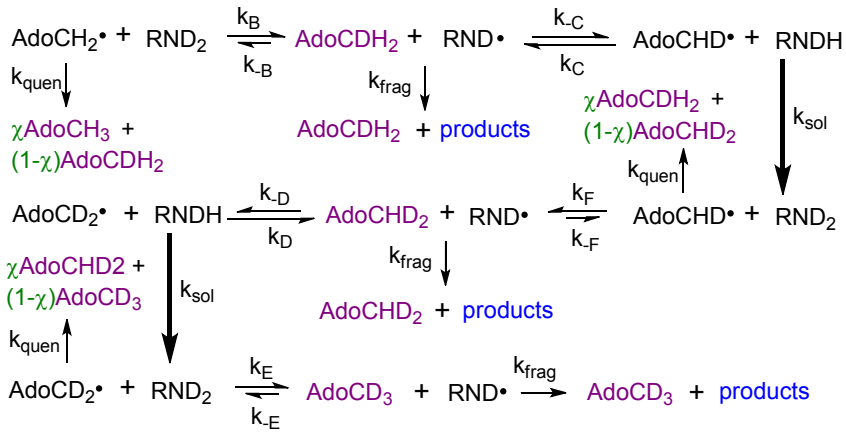

According to our calculations (**Fig. S12** and **Table S1**), the rate constants for the dAdo radical-based protium transfer is generally 10～12 folds higher than those of deuterium transfer, and the secondary deuterium kinetic isotope effect is small, meaning that $k_{-C} \approx k_{-D} >> k_{-B} \approx k_{-F} \approx k_{-E}$, and $k_B \approx k_F \approx k_E$. To simplify our analysis, we define $k_p = k_C \approx k_D$ (p represents protium abstraction), $k_{rp} = k_{-C} \approx k_{-D}$ (rp represents reverse protium abstraction, ***k_{rp}* equals to *k_2* in Fig. 4b in the main text**), $k_d = k_B \approx k_F \approx k_E$ (d represents deuterium abstraction, ***k_d* equals to *k_1* in Fig. 4b**

in the main text), $k_{rd} = k_{-B} \approx k_{-F} \approx k_{-E}$ (rd represents reverse deuterium abstraction). The observation that dAdoH is mainly tri-deuterated in the rapid quench experiment (Fig. 4a in the main text) suggests that i) the rates for deuterium transfer is much larger than k_{quen} and k_{frag}, and ii) the Tyr90-mediated solvent exchange process should be very fast (*i.e.* $k_{sol} >> k_p$). Together, the rate constants in NosL reaction in D_2O can be ranked as follows.

$$k_{sol} >> k_p > k_{rp}\ (k_2 \text{ in Fig. 4b}) >> k_d\ (k_1 \text{ in Fig. 4b}) > k_{rd} >> k_{quen},\ k_{frag}$$

We define D_i (i = 0, 1, 2, 3) as the ratio of the yield of the dAdoH containing i deuterium atom(s) to the total yield of dAdoH (*i.e.* $\sum D_i = 1$). According to the analysis above, the ratio of mono-deuterated dAdoH (D_1) can be roughly estimated as follows.

$$D_1 \approx \frac{k_{quen}}{k_{quen} + k_d} \times (1 - \chi) + \frac{k_d}{k_{quen} + k_{quen}} \times \frac{k_{quen}}{k_{quen} + k_d} \times \chi$$

When we performed the assay in 98% D_2O with all the required reaction components except L-Trp, the results showed that the resulting dAdoH consists of ~60% of unlabeled species and ~40% of mono-deuteriated product, and this ratio remains roughly constant at different time points, suggesting that only part of the dAdo radical was quenched by solvent-exchangeable hydrogen, and **we here roughly estimate that χ is ~0.6**. Together with the results discussed in the main text showing that $\boldsymbol{D_1 \approx 0.1}$ (Fig. 4a in the main text), these analyses allow us to estimate that $\boldsymbol{k_{quen} : k_d \approx 1 : 9}$. Because k_{rp} (k_{-D}) is far larger than k_{frag}, most of the di-deuterated dAdoH should come from $AdoCD_2$•, therefore we can estimate the ratio of D_2 to D_3 as follows.

$$D_2/D_3 \approx \frac{k_{quen} \times \chi}{k_{quen} \times (1 - \chi) + \frac{k_E}{k_{-E}} k_{frag}}$$

Based on the calculation that k_E/k_{-E} is 2.6 (**Table S1**), χ is ~0.6, and D_2/D_3 is ~0.8 (Fig. 4a in the main text), we can know that $\boldsymbol{k_{frag} : k_{quen} : k_d \approx 1 : 7.5 : 67}$. Because k_d is around 5~7 s^{-1} (**Table S1**), the rate constant for the cleavage of the tryptophanyl radical 1 in NosL catalysis **($\boldsymbol{k_{frag}}$) can be estimated to be ~ 0.1 $\boldsymbol{s^{-1}}$**. It should be noted that because of the inevitable error in DFT calculations, **the rate constants inferred here are only rough estimations and should be treated cautiously;**[19] yet they do provide a general view into the complicate process of NosL-catalyzed reaction.

Fig. S12. Model hydrogen transfer reactions, which are relevant to NosL catalysis discussed in **Fig. S11** (*e.g.* k_B' and k_{-B}' are consistent with k_B and k_{-B} in **Fig. S11**). These reactions serve as models for our DFT and statistical mechanics calculations, and the resulting rate constants and thermodynamic parameters are listed in **Table S1**.

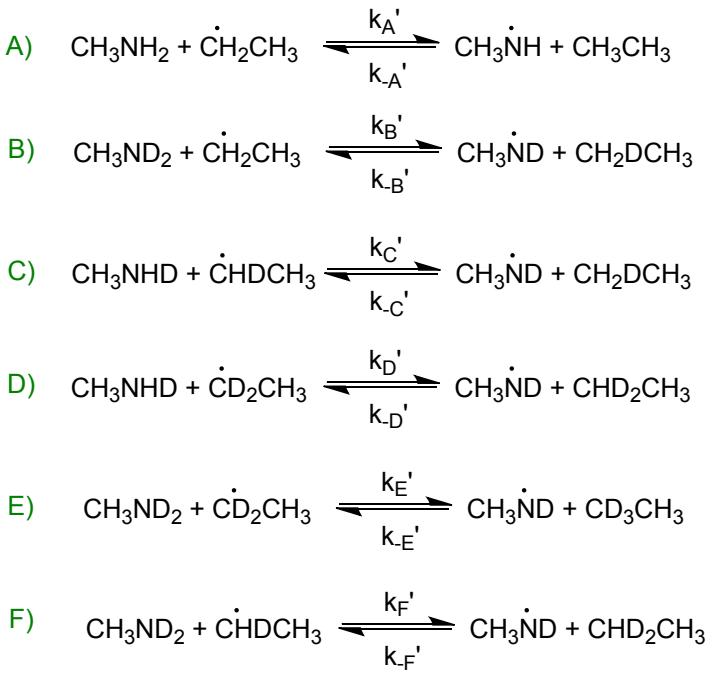

Fig. S13. Active site of NosL. The L-Trp amino group is shown by a red arrow. Hydrogen atoms were added to the repaired crystal structures at physiological pH (7.4) with the PROPKA[16] tool to optimize the hydrogen bond network provided by the Protein Preparation tool in Schrodinger software.

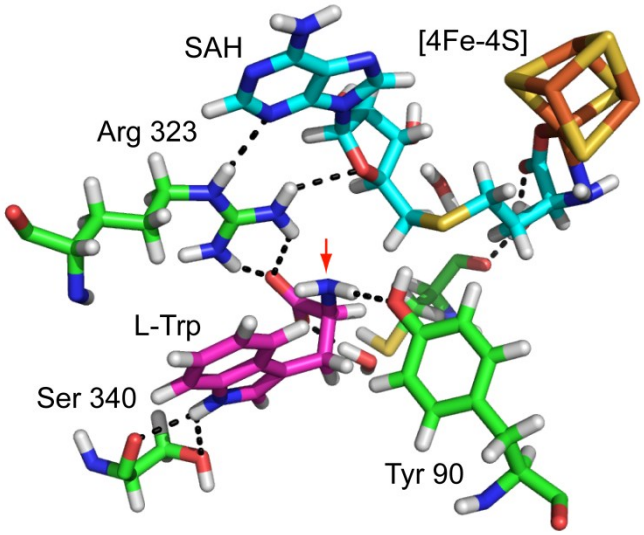

Fig. S14. Kinetic analysis of NosL wild type enzyme and the Y90F mutant for dAdoH production. The assays were performed with (a) 11 μM and (b) 33 μM enzyme in 50 mM MOPS buffer (pH 8.0) with 10 mM DTT, 200 μM L-Trp, and 2 mM sodium dithionite. The reactions were initiated by addition of SAM to the final concentration of 50 μM, 200 μM or 1mM. The reactions were quenched at 2 min by addition of trichloroacetic acid (TCA) to a final concentration of 5% (v/v). Production of dAdoH were quantified by HPLC using 5′-chloro-5′-deoxyadenosine as an internal standard, and the reactions were performed in duplicate. According to this analysis, the Km values of SAM are far smaller than 50 μM and were not measured. The result shows that the catalytic efficiency of the Y90F mutant is about 2-fold lower than the wild type enzyme; similar observations were also made by Begley and coworkers.[20]

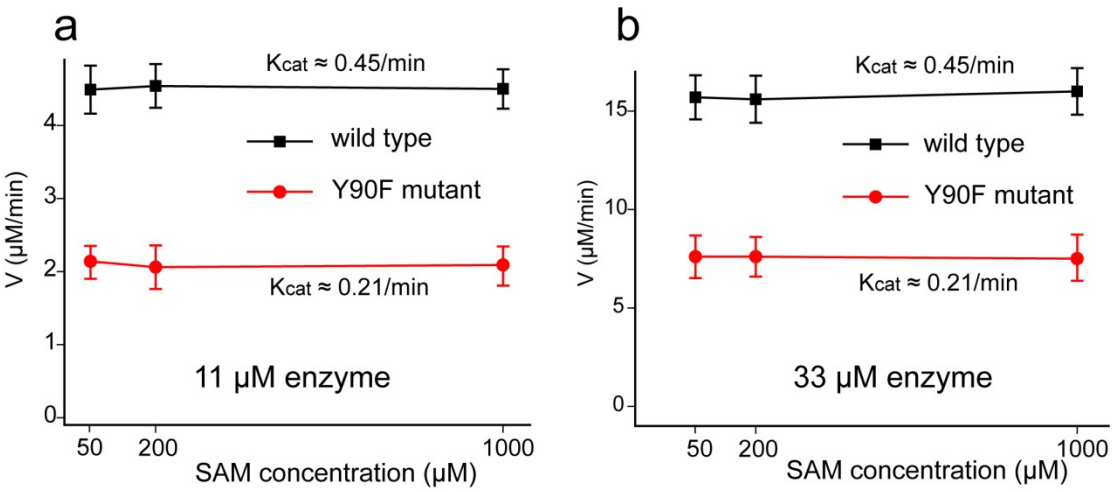

Table S1. Computational analysis of the model hydrogen transfer reactions that mimic the dAdo radical-mediated hydrogen abstraction in NosL catalysis. R_i, TS_i, and P_i refer to the reactants, transition-state, and products of the reaction i (see **Fig. S12**). DFT calculations were performed at the M06/6-311+G(2d,p)/SMD(water) level of theory. Statistical mechanics analysis were performed using the canonical transition-state theory (TST)[12] with Wigner tunneling correction (TSTW)[13] embedded in the KiSThelP software package.[14] The temperature was set to 298.00K and the atmospheric pressure to 1.0 bar without any artificial adjustment. Considering the equivalent concentration of the reactants (*i.e.* hydrogen donor and acceptor), the hydrogen transfer processes were treated as unimolecular reactions for rate constant calculation.

Reaction	k (s^{-1})	Ea (kJ/mol)	ΔG (kJ/mol)	k_i/k_{-i}	ΔΔG (kJ/mol)
$R_A \rightarrow TS_A$	54.393	44.24	67.17	2.6300	-2.40
$P_A \rightarrow TS_A$	20.682	52.88	69.57		
$R_B \rightarrow TS_B$	4.6749	49.21	72.11	1.6122	-1.18
$P_B \rightarrow TS_B$	2.8997	56.47	73.29		
$R_C \rightarrow TS_C$	63.473	43.44	66.78	2.6290	-2.39
$P_C \rightarrow TS_C$	24.143	52.3	69.17		
$R_D \rightarrow TS_D$	72.562	42.79	66.44	3.1939	-2.87
$P_D \rightarrow TS_D$	22.719	52.54	69.31		
$R_E \rightarrow TS_E$	6.6043	47.7	71.23	2.6249	-2.39
$P_E \rightarrow TS_E$	2.516	57.07	73.62		
$R_F \rightarrow TS_F$	5.7793	48.36	71.57	2.1292	-1.87
$P_F \rightarrow TS_F$	2.7143	56.76	73.44		
$R_G \rightarrow TS_G$	0.22678	67.36	79.44	0.5789	1.35
$P_G \rightarrow TS_G$	0.39176	65.14	78.09		
$R_H \rightarrow TS_H$	2.3657	62.25	74.72	1.0001	0.00
$P_H \rightarrow TS_H$	2.3654	62.25	74.72		

References

1. X. Ji, Y. Li, W. Ding and Q. Zhang, *Angew Chem Int Ed Engl*, 2015, **54**, 9021-9024.
2. H. P. and W. Kohn, *Phys. Rev.*, 1964, **136**, B864.
3. W. Kohn and L. J. Sham, *Phys. Rev.*, 1965, **140**, A1133.
4. M. J. Frisch, G. W. Trucks, H. B. Schlegel, G. E. Scuseria, M. A. Robb, J. R. Cheeseman, G. Scalmani, V. Barone, B. Mennucci, G. A. Petersson and M. C. H. Nakatsuji, X. Li, H. P. Hratchian, A. F. Izmaylov, J. Bloino, G. Zheng, J. L. Sonnenberg, M. H, ada, M. Ehara, K. Toyota, R. Fukuda, J. Hasegawa, M. Ishida, T. Nakajima, Y. Honda, O. Kitao, H. Nakai, T. Vreven, J. A. Montgomery, Jr., J. E. Peralta, F. Ogliaro, M. Bearpark, J. J. Heyd, E. Brothers, K. N. Kudin, V. N. Staroverov, R. Kobayashi, J. Normand, K. Raghavachari, A. Rendell, J. C. Burant, S. S. Iyengar, J. Tomasi, M. Cossi, N. Rega, J. M. Millam, M. Klene, J. E. Knox, J. B. Cross, V. Bakken, C. Adamo, J. Jaramillo, R. Gomperts, R. E. Stratmann, O. Yazyev, A. J. Austin, R. Cammi, C. Pomelli, J. W. Ochterski, R. L. Martin, K. Morokuma, V. G. Zakrzewski, G. A. Voth, P. Salvador, J. J. Dannenberg, S. Dapprich, A. D. Daniels, Ö. Farkas, J. B. Foresman, J. V. Ortiz, J. Cioslowski, and D. J. Fox, *Gaussian 09, Revision E.01, Gaussian, Inc., Wallingford CT, 2009.*, 2009.
5. C. Lee, W. Yang and R. G. Parr, *Phys. Rev.*, 1988, **B37**, 785.
6. A. D. Becke, *J. Chem. Phys.*, 1993, **98**, 5648-5652.
7. Y. Zhao and D. G. Truhlar, *Theor Chem Acc*, 2008, **120**, 215-241.
8. M. T. Cances, B. Mennucci and J. Tomasi, *J. Chem. Phys.*, 1997, **107**, 3032.
9. M. Cossi, V. Barone, B. Mennucci and J. Tomasi, *Chem. Phys. Lett.* , 1998, **286**, 253.
10. A. V. Marenich, C. J. Cramer and D. G. Truhlar, *J Phys Chem B*, 2009, **113**, 6378-6396.
11. R. Rohac, P. Amara, A. Benjdia, L. Martin, P. Ruffie, A. Favier, O. Berteau, J. M. Mouesca, J. C. Fontecilla-Camps and Y. Nicolet, *Nat Chem*, 2016, **8**, 491-500.
12. H. Eyring, *J Chem Phys*, 1935, **3**, 107-115.
13. D. G. Truhlar and R. E. Wyatt, *Annu Rev Phys Chem*, 1976, **27**, 1-43.
14. S. Canneaux, F. Bohr and E. Henon, *J Comput Chem*, 2014, **35**, 82-93.
15. D. Shivakumar, J. Williams, Y. J. Wu, W. Damm, J. Shelley and W. Sherman, *J Chem Theory Comput*, 2010, **6**, 1509-1519.
16. C. R. Sondergaard, M. H. M. Olsson, M. Rostkowski and J. H. Jensen, *J Chem Theory Comput*, 2011, **7**, 2284-2295.
17. Z. S. Li, W. M. Wang, W. Lu, C. W. Niu, Y. H. Li, Z. M. Li and J. G. Wang, *Bioorg Med Chem Lett*, 2013, **23**, 3723-3727.
18. W. R. Bowman, M. J. Broadhurst, D. R. Coghlan and K. A. Lewis, *Tetrahedron Lett*, 1997, **38**, 6301-6304.
19. F. Himo, *Biochim Biophys Acta* , 2005, **1707**, 24-33.
20. D. M. Bhandari, H. Xu, Y. Nicolet, J. C. Fontecilla-Camps and T. P. Begley, *Biochemistry*, 2015, **54**, 4767-4769.